

Thierry Bodineau · Vivien Lecomte ·
Cristina Toninelli

Finite size scaling of the dynamical free-energy in a kinetically constrained model

December 30, 2017

Abstract We determine the finite size corrections to the large deviation function of the activity in a kinetically constrained model (the Fredrickson-Andersen model in one dimension), in the regime of dynamical phase coexistence. Numerical results agree with an effective model where the boundary between active and inactive regions is described by a Brownian interface.

Contents

1	Introduction	2
1.1	The large deviation function and its singularities	2
1.2	Finite size scaling of the large deviation function	3
2	Model and description of the coexistence of active and inactive regions	3
2.1	Large deviations of the activity in the Fredrickson-Andersen model	3
2.2	Finite-size scaling and an interface model	4
3	Numerical results	6
3.1	Results from the cloning algorithm (1): the free energy	6
3.2	Results from the cloning algorithm (2): the density	7
3.3	Results in an independent site approximation	8
4	Discussion	10
4.1	Determination of the effective jump rates p and q , and the surface tension Σ	10
4.2	Universality	11
4.3	Finite size scaling of the large deviation function $\pi_L(k)$	11
5	Conclusion	14
A	Scaling of $\psi_L(s)$ in the interface model	15
B	A generic identity between large deviation functions	16
C	Bernoulli approximation to determine $\varphi_L(\lambda)$	17

Thierry Bodineau
École Normale Supérieure, DMA, 45 rue d'Ulm 75230 Paris cedex 05, France,
Vivien Lecomte · Cristina Toninelli
Laboratoire Probabilités et Modèles Aléatoires, UMR CNRS 7599, Universités Paris VI et
Paris VII, site Chevaleret, 175 rue du Chevaleret, 75013 Paris, France

1 Introduction

Glassy phenomena have proven difficult to understand: they present a variety of features – slow dynamics, ageing, dynamical heterogeneity, frustration – which make their study arduous from a theoretical point of view (see [1] for a recent review). Kinetically Constrained Models (KCMs) are a simple class of lattice gases whose dynamics shares features similar to those of glassy phenomena, with the advantage that no disorder is present in the model – which makes them easier to study (see [2,3] for reviews on KCMs).

There is a variety of KCMs (see section 2.1 for a concrete example) which all share a common feature: their static properties are trivial and their complexity (like the phase transition phenomena) is hidden in their dynamical behaviour. This raises the problem of finding relevant physical parameters in order to describe and classify the properties of these models. As the glassy systems are characterised by a mixture of frozen and mobile areas, the “activity” of the system (namely the number of local updates during a time interval) has been proposed as a relevant dynamical parameter and a dynamical approach has been recently devised in order to define a suitable notion of dynamical free energy [4,5,6,7,8]. In this dynamical framework, the role of the free energy is played by the large deviation function of the activity.

1.1 The large deviation function and its singularities

For lattice gases (or more generically for Markov process with discrete configuration space) with continuous-time dynamics, the simplest definition of the activity is the number of configuration changes presented by an history of duration t [4,9] (see [10,11,12] for alternative definitions in systems with continuous degree of freedom). For each history of duration t of the system, the activity will be denoted by the observable K_t . KCMs and other glassy systems present “dynamical heterogeneities” [13], *i.e.* regions which remain frozen during a long time. This feature can be captured by the probability distribution function of the activity as some histories present slow or inactive intervals with higher probability than in non-glassy systems. In the large-time limit, the probability of observing an atypical value $K_t = kt$ of the activity scales as

$$\text{Prob}[K_t = kt] \underset{t \rightarrow \infty}{\sim} e^{t\pi(k)}$$

In the infinite size limit, the function $\pi(k)$ may no longer be analytic. This can be interpreted as a signature of the dynamical heterogeneities [4,14]. We postpone a more quantitative discussion of the singularities to section 4.3.

From a practical point of view, it proves in fact easier to make a Laplace transform and consider instead [5]

$$\langle e^{-sK_t} \rangle \underset{t \rightarrow \infty}{\sim} e^{t\psi(s)}$$

where the average is taken over histories of duration t . The parameter s plays a role similar to the inverse temperature in the canonical ensemble of equilibrium statistical mechanics: fixing s boils down to fixing the average value of the activity, in the same way as fixing the temperature determines the average energy. The functions $\psi(s)$ and $\pi(k)$ are related by a Legendre transform: $\psi(s) = \sup_k \{\pi(k) - sk\}$.

It has been shown for several KCMs that $\psi(s)$ presents a singularity at $s \downarrow 0$ in the infinite size limit, which corresponds to a dynamical phase coexistence

between active histories (at $s \leq 0$) and inactive histories (at $s > 0$) [6,7], in the same way as singularities of the free energy correspond to transition phases in equilibrium statistical mechanics. Similar singularities have been observed in other glassy systems (see [10,12] for binary Lennard-Jones mixtures), but the question of finding a generic relation between glassy properties which hold at $s = 0$ and the singularity of $\psi(s)$ is still open. Indeed, for any finite size system the cumulants of the activity: $\frac{1}{t} \langle K_t^n \rangle_c = (-1)^n \partial_s^n \psi(s)|_{s=0}$ can be obtained from the function $\psi(s)$, but this correspondence does not hold in the infinite size limit and one may wonder if the singularity of ψ at $s = 0$ has an impact for the physics of finite size dynamics. Thus it is a natural question to understand how this singularity is build up when the system size diverges and in this article we are interested in the finite-size scaling of the large deviation function $\psi(s)$, especially around the transition.

1.2 Finite size scaling of the large deviation function

It has been shown that finite-size effects capture non-trivial physical features of the typical configurations of the system giving rise to the atypical deviation, such as the stationarity or the stability of the density profile in one-dimensional transport systems [15,16,17] or the geometrical features of the system configurations in glassy systems [8,12]. From a broader point of view, other quantities than the activity (such as the time and space integrated current) present a large deviation function which becomes singular in the infinite size limit [16,18,19], also describing a dynamical phase transition.

2 Model and description of the coexistence of active and inactive regions

2.1 Large deviations of the activity in the Fredrickson-Andersen model

We focus on a one-dimensional version of the Fredrickson-Andersen [20] model (FA model), in periodic boundary conditions. It consists of a lattice of size L described by occupation numbers $\mathbf{n} = (n_i)_{1 \leq i \leq L}$ with sites 0 and L identified. Each site i is either occupied (or ‘active’, $n_i = 1$) or empty (or ‘inactive’, $n_i = 0$). Transition rates are

$$W(n_i = 0 \rightarrow n_i = 1) = c C_i \quad (1)$$

$$W(n_i = 1 \rightarrow n_i = 0) = (1 - c) C_i \quad (2)$$

with $C_i = n_{i-1} + n_{i+1}$. The kinetic constraint C_i encodes the ‘‘dynamical facilitation’’ rule: active regions favour activity in their vicinity. Compared to the unconstrained system ($C_i = 1$), the kinetic constraint does not modify the steady equilibrium state: each site has a Poissonian occupation number of density c , excepted that the configuration where all sites are inactive is dismissed. The kinetic constraint however modifies the dynamical relaxation of correlation functions [20] with features similar to those of glassy systems.

It has been shown that the dynamical free energy $\psi_L(s)$ of a system of size L , defined as

$$\langle e^{-sK_t} \rangle \underset{t \rightarrow \infty}{\sim} e^{t\psi_L(s)} \quad (3)$$

presents a first order transition in the infinite size limit [6, 7]:

$$\frac{1}{L}\psi_L(s) \xrightarrow{L \rightarrow \infty} \begin{cases} > 0 & \text{if } s \leq 0 \\ 0 & \text{if } s > 0 \end{cases} \quad (4)$$

Note that the mean activity $\frac{1}{t}\langle K_t \rangle_s = \frac{\langle K_t e^{-sK_t} \rangle}{t\langle e^{-sK_t} \rangle}$, is also $\frac{1}{t}\langle K_t \rangle_s = -\psi'_L(s)$. The transition can be interpreted as follows:

- $s < 0$ corresponds to histories where the mean activity $\langle K_t \rangle_s$ is larger than the typical one. For these histories, the number of active sites remains extensive with the system size.
- $s > 0$ corresponds to histories where the mean activity $\langle K_t \rangle_s$ is smaller than the typical one. For these histories, the number of active sites becomes finite in the large size limit. In particular for infinite s the value of the large deviation function is given by (the opposite of) the escape rate with only one active site in the system [7]:

$$\lim_{s \rightarrow \infty} \lim_{L \rightarrow \infty} \psi_L(s) = -r_\infty \equiv -2c \quad (5)$$

2.2 Finite-size scaling and an interface model

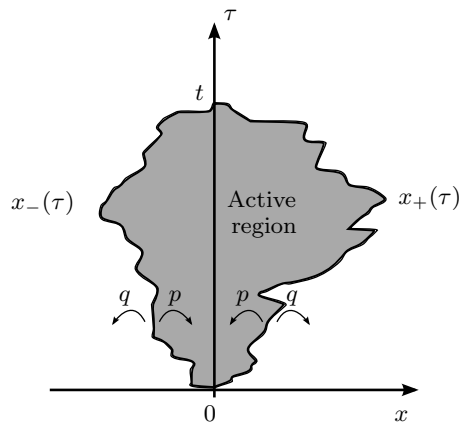


Fig. 1: Model for the space-time configuration of the system in the interfacial regime $\lambda > \lambda_c$. An island of activity density $\mathbb{K} = 4c^2(1 - c)$ is delimited by two non-crossing biased random walks $x_+(\tau)$ and $x_-(\tau)$, constrained to start at 0 and end at 0 at time t .

In [8] two of the authors have considered a different scaling regime by focusing on values of s of the order $s = \lambda/L$ and for the function

$$\varphi_L(\lambda) \equiv \psi_L(\lambda/L) \quad (6)$$

they conjectured that there exists a critical value $\lambda_c > 0$ of λ such that

$$\varphi(\lambda) = \lim_{L \rightarrow \infty} \varphi_L(\lambda) = \begin{cases} -\mathbb{K}\lambda & \text{for } \lambda \leq \lambda_c \\ -\Sigma & \text{for } \lambda \geq \lambda_c \end{cases} \quad (7)$$

where $\mathbb{K} = \frac{1}{Lt} \langle K_t \rangle = 4c^2(1-c)$ is the mean average activity in the system, and Σ is the surface tension accounting for the cost of maintaining an interface between an active and an inactive region in the system for a long time. In [8], the limit (7) was derived only in a range of values $\lambda < \lambda_0$ and $\lambda > \lambda_1$ for some parameters $0 < \lambda_0 < \lambda_1$ and not up to the conjectured critical value $\lambda_c = \frac{\Sigma}{\mathbb{K}}$.

Note that $\Sigma \neq r_\infty$: the typical configurations of the system at finite $\lambda > \lambda_c$ are not given by those of the $s \rightarrow \infty$ limit. In particular, they present more than a finite number of active sites. Our aim in this article is to identify the typical configurations occurring at $\lambda > \lambda_c$, and to determine the finite size corrections that they imply on the infinite size result (7). These configurations are interesting to characterise because they are the first to appear when increasing λ (that is, they are the first to appear when considering histories of the system displaying an activity K_t lower than the typical one).

We introduce now a simplified dynamics in order to model the configurations at $\lambda > \lambda_c$. In the slow activity regime, the system can be described at a macroscopic level by a small active “island” of mean activity \mathbb{K} in a large sea of an inactive region (see figure 1). In the unbiased dynamics ($\lambda = 0$), the inactive region would be invaded and become active. Thus at the macroscopic level, an interface between an active and an inactive region should perform a biased random walk with effective jump rates p, q which take into account the growth of the active region. When $\lambda > \lambda_c$, the growth of the active region is penalised as the activity of the system is proportional to the area of the active droplet.

More precisely, the boundaries $x_+(t)$ and $x_-(t)$ of the active region perform non-crossing random walks of jump rate p (resp. q) to the left (resp. right) for $x_+(t)$ and mirror rates for $x_-(t)$. For simplicity the walks are constrained to start from $x = 0$ at time 0, and to come back to 0 at final time t (this assumption does not change the large time asymptotics). In this effective description, the total activity in the system is proportional to the area of the active droplet and approximated by $\mathbb{K} \int_0^t d\tau [x_+(\tau) - x_-(\tau)]$ with $\mathbb{K} = 4c^2(1-c)$ the mean density of activity. Thus the counterpart of $\langle e^{-sK_t} \rangle$ reads

$$Z_{\text{eff}}(s, t) \equiv \frac{\left\langle e^{-s\mathbb{K} \int_0^t d\tau [x_+(\tau) - x_-(\tau)]} \delta(x_\pm(t) = 0) \right\rangle_{p,q}}{\left\langle \delta_\pm(x(t) = 0) \right\rangle_{p,q}} \quad (8)$$

where $\langle \cdot \rangle_{p,q}$ denotes the average over trajectories $x_\pm(\tau)_{0 \leq \tau \leq t}$ without constraint at final time.

This is the simplest model one can think of to represent the separation between active and inactive regions in the system. In particular adding more interfaces would lead to a metastable situation where the active regions eventually merge together to form a unique island of activity. We think that the interface model represents the correct dynamics of the system at large scale, but we have not found a rigorous derivation starting from the microscopic dynamics. However, the numerical results of section 3 support the scaling derived from the simplified model (11).

Thus we conjecture that the finite size corrections to the large deviation function $\varphi_L(\lambda)$ (6) for $\lambda > \lambda_c$ are related to

$$\hat{\varphi}_L(\lambda) = \lim_{t \rightarrow \infty} \frac{1}{t} \log Z_{\text{eff}}\left(\frac{\lambda}{L}, t\right) \quad (9)$$

Inspired by the study of interfaces in the static Ising model [21, 22], and using results from Brownian bridge theory [23], we show in appendix A that this leads

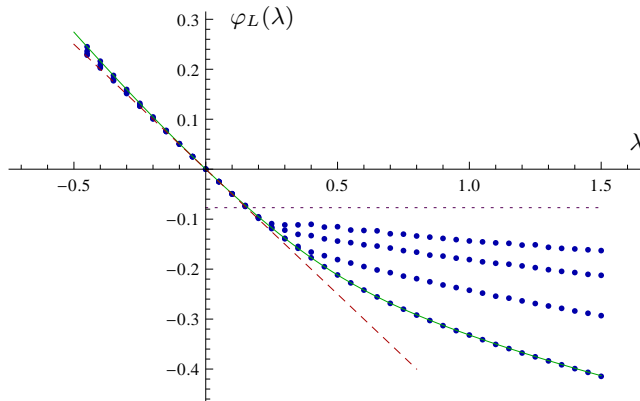


Fig. 2: Evaluation of the large deviation function $\varphi_L(\lambda)$ using the cloning algorithm (blue circles, increasing sizes $L \in \{8, 16, 32, 64\}$ from bottom to top at positive λ), and using direct diagonalisation of the operator of evolution (54) (plain green line, $L = 8$ run as a check). The red dashed line is the infinite L result $-\mathbb{K}\lambda$ for $\lambda < \lambda_c$, while the purple dotted horizontal line is the infinite L result $-\Sigma$ for $\lambda > \lambda_c$. We took $c = \frac{1}{2}$.

to the following scaling at large L

$$\hat{\varphi}_L(\lambda) = -4\sqrt{pq} \left(\frac{\lambda\mathbb{K}}{4L\sqrt{pq}} \right)^{\frac{2}{3}} 2^{-\frac{1}{3}}\alpha_1 \quad (10)$$

where $\alpha_1 \approx 2.3381\dots$ is the first zero of the Airy function on the negative real axis. As a consequence, we expect that the finite size scaling of the microscopic model should be given by (10) plus the extra cost $-\Sigma$ for creating the interfaces

$$\varphi_L(\lambda) = -\Sigma - 4\sqrt{pq} \left(\frac{\lambda\mathbb{K}}{4L\sqrt{pq}} \right)^{\frac{2}{3}} 2^{-\frac{1}{3}}\alpha_1 \quad (11)$$

for appropriate choice of the effective parameters p, q (see section 4.1 for a discussion on the effective jump rates). In other words the interface model we have considered leads to $L^{-\frac{2}{3}}$ corrections to the constant $-\Sigma$.

3 Numerical results

3.1 Results from the cloning algorithm (1): the free energy

To investigate whether the finite size corrections (11) inferred from the interface model are correct, we have measured $\varphi_L(\lambda)$ in numerical simulations. Since large deviations are by definition difficult to measure, a direct sampling of $\psi_L(s)$ through (3) is not achievable. We have resorted to a continuous-time version [24, 25] of the Giardinà-Kurchan-Peliti cloning algorithm [26] in which the dynamics is modified so as to make the large deviation typical, at the price of mutation/selection rules between a large number of copies of the system (see [27] for a review on cloning algorithms). Those algorithms have already been used to determine large deviation functions in lattice gases [6, 28, 29] but not in the scaling regime $s = \lambda/L$ that we consider in this article.

A first result (figure 2) is that the large deviation function agrees qualitatively with the conjectured infinite size result (7): the large deviation function $\varphi_L(\lambda)$

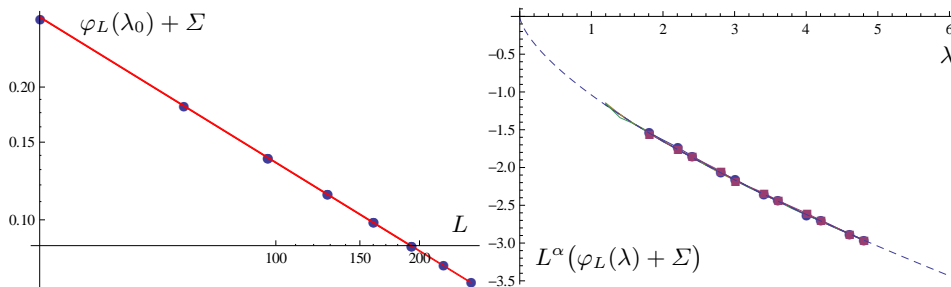


Fig. 3: **(Left)** Log-log plot of $\varphi_L(\lambda_0) + \Sigma$, for $\Sigma = 0.077$, at fixed $\lambda_0 = 4.6$ as a function of L : the numerical evaluation (blue dots) fits with a power law corresponding to the exponent $\alpha = \frac{2}{3}$ (red line). **(Right)** Plot of $L^\alpha(\varphi_L(\lambda) + \Sigma)$ for different values of L ($L \in \{64, 96, 128, 160, 192, 256, 320\}$). The curves collapse on a single master curve $-1.05\lambda^\alpha$ (dashed blue), in agreement with the interfacial model result (11). The parameter c of the model is $c = \frac{1}{2}$.

tends to become linear for $\lambda < \lambda_c$ and constant for $\lambda > \lambda_c$ as L increases. The critical value is determined as $\lambda_c = \Sigma/\mathbb{K}$.

The scaling of the deviations from the infinite size result is examined in figure 3. In agreement with the interfacial model result (11), $\varphi_L(\lambda) + \Sigma$ scales in $L^{-\alpha}$ at fixed λ (figure 3, left), with $\alpha = \frac{2}{3}$, while the rescaled curves $L^\alpha(\varphi_L(\lambda) + \Sigma)$ collapse onto a master curve $-A_1\lambda^\alpha$, with $A_1 \simeq 1.04$ (figure 3, right). Simulations were performed at mean density $c = \frac{1}{2}$, but the results and the scaling analysis we present do not depend on this value.

3.2 Results from the cloning algorithm (2): the density

One may test another consequence of the interfacial model by computing the density of active sites. Taking the derivative with respect to s in (3) leads to $\frac{1}{t}\langle K_t \rangle_s = -\psi'_L(s)$. Thus using the relation (6) implies that $\frac{1}{t}\langle K_t \rangle_\lambda = -L\varphi'_L(\lambda)$ and from (11) the mean activity $\frac{1}{t}\langle K_t \rangle_\lambda$ for histories weighted by $e^{-\lambda K_t/L}$ scales as $L^{\frac{1}{3}}$. Therefore, one expects that the average width of the active droplet is $L^{\frac{1}{3}}$ when $\lambda > \lambda_c$. Strong finite-size effects are still present (figure 4) and wouldn't allow to check precisely the power $\frac{2}{3}$ of the scaling relation (11). To understand the origin of these corrections a useful tool is the escape rate $r(\mathcal{C})$ from a configuration $\mathcal{C} = (n_i)_{1 \leq i \leq L}$ defined as the sum of the jump rates from \mathcal{C} : $r(\mathcal{C}) = \sum_{i=1}^L [(1-c)n_i + c(1-n_i)](n_{i-1} + n_{i+1})$. As shown in appendix B, the fluctuations of K_t and of the time integral of the escape rate $R_t = \int_0^t d\tau r(\mathcal{C}(\tau))$ are closely related (this result is valid in general):

$$\psi_L(s) = \frac{1}{t}\langle K_t \rangle_s - \frac{1}{t}\langle R_t \rangle_s \quad (12)$$

In the interfacial regime $\lambda > \lambda_c$, $\varphi_L(\lambda)$ goes to a constant $-\Sigma$ when L goes to infinity, while both $\frac{1}{t}\langle K_t \rangle_\lambda$ and $\frac{1}{t}\langle R_t \rangle_\lambda$ grow with L so that (12) describes the cancellation between those growths. More precisely, assuming the scaling form

$$\varphi_L(\lambda) = -\Sigma + L^{-\alpha}\varphi^1(\lambda) + o(L^{-\alpha}) \quad (13)$$

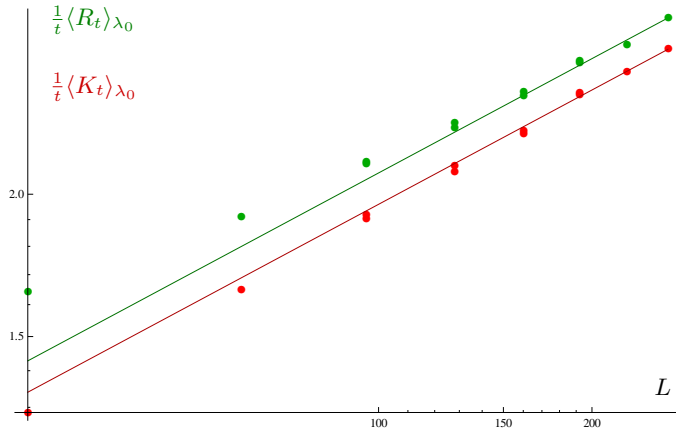


Fig. 4: In red (resp. green): log-log plot of $\frac{1}{t}\langle K_t \rangle_{\lambda_0}$ (resp. $\frac{1}{t}\langle R_t \rangle_{\lambda_0}$) at fixed $\lambda_0 = 4.6$ as a function of L (same values as in figure 3). Dots are numerical data while lines are power law asymptotics with exponent $1 - \alpha = \frac{1}{3}$. Duplicated dots correspond to different runs.

one sees by differentiating (12) that both $\langle K_t \rangle_{\lambda}$ and $\langle R_t \rangle_{\lambda}$ scale in the same way with L

$$\frac{1}{t}\langle K_t \rangle_{\lambda} \sim L^{1-\alpha} k_1(\lambda) + o(L^{1-\alpha}) \quad \frac{1}{t}\langle R_t \rangle_{\lambda} \sim L^{1-\alpha} r_1(\lambda) + o(L^{1-\alpha}) \quad (14)$$

where the exponent $1 - \alpha$ comes from the relation $\frac{1}{t}\langle K_t \rangle_{\lambda} = -L\varphi'_L(\lambda)$ and $r_1 = k_1$.

We also note that at $c = \frac{1}{2}$, $r(C)$ is (twice) the total number of active sites so that the $\frac{1}{t}\langle R_t \rangle_{\lambda}$ also represents the mean density of active sites at fixed λ , which thus scales as $L^{1-\alpha} = L^{\frac{1}{3}}$ (we expect the result to hold also for $c \neq \frac{1}{2}$ although $\frac{1}{t}\langle R_t \rangle_{\lambda}$ is not the mean density anymore). We conclude that a numerical check or evaluation of the exponent α is better done on $\varphi_L(\lambda)$ than on the mean activity, the density or the escape rate, since those quantities present large finite-size corrections *e.g.* of the form

$$\frac{1}{t}\langle K_t \rangle_{\lambda} \sim L^{1-\alpha} k_1(\lambda) + L^{\gamma} k_2(\lambda) + C_K + O(L^{-\alpha}) \quad (15)$$

$$\frac{1}{t}\langle R_t \rangle_{\lambda} \sim L^{1-\alpha} r_1(\lambda) + L^{\gamma} r_2(\lambda) + C_R + O(L^{-\alpha}) \quad (16)$$

where by cancellation from (12) $k_1 = r_1$, $k_2 = r_2$ and $C_K - C_R = -\Sigma$.

3.3 Results in an independent site approximation

We now consider another approach to compute the dynamical free energy $\varphi_L(\lambda)$. It can be shown that $\varphi_L(\lambda)$ is the largest eigenvalue of a symmetric operator of evolution $\mathbb{W}_{\lambda}^{\text{sym}}$ [5] (see also appendices B and C) which acts on the vector space of all configurations $\{\mathbf{n}\}$ of the system. We thus have the Courant-Fisher equality

$$\varphi_L(\lambda) = \max_{|X\rangle \neq 0} \frac{\langle X | \mathbb{W}_{\lambda}^{\text{sym}} | X \rangle}{\langle X | X \rangle} \quad (17)$$

where $|X\rangle = \sum_{\mathbf{n}} X(\mathbf{n})|\mathbf{n}\rangle$ is a vector.

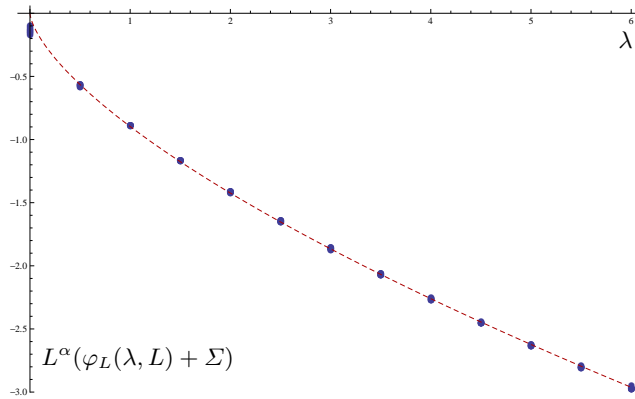


Fig. 5: Plot of the scaling function $L^\alpha(\varphi_L(\lambda, L) + \Sigma)$ for different values of L ($L \in \{32, 36, 40, \dots, 96, 100\}$) determined from the Bernoulli optimisation (18) (blue dots). The curves collapse on a single master curve $-A_1\lambda^\alpha$ (dashed red). The values of Σ and A_1 are quite different from those of the original FA model: here, $\Sigma \approx 0.251$ and $A_1 \approx 0.897$.

Restricting the optimisation on laws $X(\mathbf{n})$ representing products of Bernoulli distributions for evaluating the largest eigenvalue of $\mathbb{W}_s^{\text{sym}}$, one obtains in appendix C the following estimation for the large deviation function: $\varphi_L(\lambda) \leq \varphi_L^{\text{Bern}}(\lambda)$ with

$$\varphi_L^{\text{Bern}}(\lambda) = \max_{\{\rho_i\}} \frac{\sum_{1 \leq i \leq L} [e^{-\lambda L} \sqrt{c(1-c)\rho_i(1-\rho_i)} - c(1-\rho_i) - (1-c)\rho_i](\rho_{i+1} + \rho_{i-1})}{1 - \prod_{1 \leq i \leq L} (1 - \rho_i)} \quad (18)$$

where $0 < \sqrt{\rho_i} < 1$ is the parameter of the Bernoulli law at site i .

The mean value of the mean fraction of active sites $\frac{1}{Lt} \int_0^t d\tau \sum_i n_i(\tau)$ for histories weighted by e^{-sKt} is given by

$$\bar{\rho}(\lambda, L) \equiv \lim_{t \rightarrow \infty} \left\langle e^{-sKt} \frac{1}{Lt} \int_0^t d\tau \sum_i n_i(\tau) \right\rangle / \langle e^{-sKt} \rangle = \langle L | \frac{1}{L} \sum_i \hat{n}_i | R \rangle \quad (19)$$

where $|L\rangle$ and $|R\rangle$ are the left and right eigenvectors of \mathbb{W}_s associated to the eigenvalue $\varphi_L(s)$. The corresponding value in the Bernoulli projection reads

$$\bar{\rho}^{\text{Bern}}(\lambda, L) = \frac{1}{L} \frac{1}{1 - \prod_{1 \leq i \leq L} (1 - \rho_i)} \sum_{1 \leq i \leq L} \rho_i \quad (20)$$

for a set $\{\rho_i\}$ which optimises (18). Numerically solving (18) one obtains $\bar{\rho}^{\text{Bern}}(\lambda, L)$ and the large deviation function. The collapse for $\varphi_L^{\text{Bern}}(\lambda)$ works again with $\alpha = \frac{2}{3}$ (see figure 5), while again $\bar{\rho}^{\text{Bern}}(\lambda, L)$ displays stronger finite-size effects.

We expect the true minimiser to be very different from the approximation by a Bernoulli distribution. Indeed the sites located at the interface should be very correlated. This explains why the values of Σ and A_1 measured within the Bernoulli approximation are different from those of the original FA model (see section 4.2).

4 Discussion

4.1 Determination of the effective jump rates p and q , and the surface tension Σ

The exponent $\alpha = \frac{2}{3}$ observed numerically matches the one predicted by the interface model (11). One can also compare the value of the coefficient A_1 in the scaling

$$\varphi_L(\lambda) = -\Sigma - A_1 \left(\frac{\lambda}{L}\right)^\alpha + o(L^{-\alpha}) \quad (21)$$

In a very crude approximation, where correlations are neglected, one can imagine the interface as a single active site at position $x(t)$ separating a region with only inactive sites from an active region sampled according to a Bernoulli measure with parameter c . In this case, the parameters p , q of the interface model defined in section 2.2 can be estimated as follows. We have $q = c$: the interface grows at rate c by activating a site on the left of $x(t)$. On the other hand, the value of p may be estimated to $p = c(1 - c)$: due to the kinetic constraint the first active site is inactivated with rate $1 - c$ provided that the site to its right is active, which occurs with probability c . From (11) and $\mathbb{K} = 4c^2(1 - c)$, this yields

$$A_1 = 4\sqrt{pq} \left(\frac{\mathbb{K}}{4\sqrt{pq}}\right)^{\frac{2}{3}} 2^{-\frac{1}{3}}\alpha_1 = \mathbb{K}^{\frac{5}{6}}\alpha_1 \quad (22)$$

and thus $A_1 \simeq 1.312$ for $c = \frac{1}{2}$. This is close to the value $A_1 \approx 1.05 \pm 0.01$ observed numerically, the discrepancy arising in part from correlations between neighbouring sites around the interface.

The value of the dynamical surface tension Σ can be compared to analytical predictions. In [8] an expression of Σ was derived for the East and the FA models with fixed boundary condition. A similar expression holds for the periodic FA model we are interested in:

$$\Sigma = - \lim_{L \rightarrow \infty} \sup_P \langle \sqrt{P} | \mathbb{W}^{\text{sym}}(L) | \sqrt{P} \rangle \quad (23)$$

where the supremum is performed over all probability distributions on the set of configurations $\{\mathbf{n}\}$ of the system, with the condition that site 1 is inactive: $n_1 = 0$. The vector $|\sqrt{P}\rangle$ is the vector of components $\sqrt{P(\mathbf{n})}$. The symmetrized operator of evolution $\mathbb{W}^{\text{sym}}(L)$ for a system of size L is defined in appendix C. Note that the formulation of this extremalisation principle in [8] involves a Dirichlet form which is equal to the expression maximised in (23), up to a sign. Defining now the projector \mathbb{P}_L onto the configurations with site 1 inactive, we can replace $\mathbb{W}^{\text{sym}}(L)$ by $\mathbb{P}_L \mathbb{W}^{\text{sym}}(L) \mathbb{P}_L$ in (23) and relax the condition on P . This shows that:

$$\Sigma = \lim_{L \rightarrow \infty} \Sigma_L \quad \text{with} \quad \Sigma_L = - \max \text{Sp} (\mathbb{P}_L \mathbb{W}^{\text{sym}}(L) \mathbb{P}_L) \quad (24)$$

where Sp denotes the spectrum of an operator. We thus have expressed the dynamical surface tension using the maximum eigenvalue of an operator, in a similar way as for the free energy $\psi_L(s)$ in (17). The value of Σ_L was computed for systems sizes $L \leq 15$ by direct diagonalisation (figure 6). By fitting the results using a reasonable form of the finite-size corrections we obtain the value $\Sigma = 0.0771$, which is numerically compatible to the one obtained from the cloning algorithm $\Sigma = 0.077 \pm 0.0005$. Note that the finite-size surface tension Σ_L displays strong finite-size effects fitted through the form $\Sigma_L = \Sigma + AL^{-\frac{5}{3}}$, but we have no theoretical justification for the power $\frac{5}{3}$.

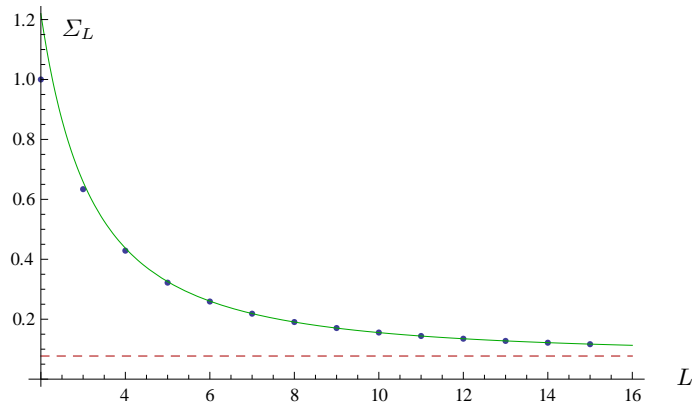


Fig. 6: Plot of the surface tension Σ_L at size L obtained by diagonalisation of the operator appearing in (24) (blue dots). To determine the surface tension $\Sigma = \lim_{L \rightarrow \infty} \Sigma_L$, we performed the fit $\Sigma_L = \Sigma + AL^{-\frac{5}{3}}$ (green line). The exponent $\frac{5}{3}$ was chosen as the most likely one in regards of the numerical results. The result $\Sigma = 0.0771$ (horizontal red dashed line) is very close from the one obtained with the cloning algorithm (0.077, see figure 3).

4.2 Universality

The Bernoulli approximation developed in part 3.3 presents the same scaling exponent $\alpha = \frac{2}{3}$ with different constants Σ and A_1 (see figure 5). This tells that, on the one hand, the independent site approximation of the Bernoulli optimisation (18) is quite far from being correct: the large deviations do not match at all. This fact was also checked by diagonalising the operator of evolution \mathbb{W}_s and finding the eigenvector associated to the maximal eigenvalue $\psi_L(s)$, for small system sizes ($L \leq 15$). We found that the corresponding state can't be factorised on independent sites and presents correlations. On the other hand, the robustness of the exponent $\frac{2}{3}$ is an indication that other models in the same class also present (an) interface(s) in the coexistence regime.

Besides, let us note that the same expression as (18) appears when considering the field theory associated to the operator of evolution $\mathbb{W}_\lambda^{\text{sym}}$ [5] and computing $\varphi_L(\lambda)$ assuming a time-independent saddle-point. This tells that such an assumption is not valid.

4.3 Finite size scaling of the large deviation function $\pi_L(k)$

At fixed system size L , the large deviation function π_L defined as

$$\text{Prob}[K_t = Lkt] \underset{t \rightarrow \infty}{\sim} e^{t\pi_L(k)} \quad (25)$$

is the Legendre transform of ψ_L (3)

$$\pi_L(k) = \inf_s \{sLk + \psi_L(s)\}, \quad \psi_L(s) = \sup_k \{-sLk + \pi_L(k)\}.$$

Using the parameter $\lambda = sL$, the large deviation function becomes, in the large L limit, for reduced activities

$$\forall k \in [0, \mathbb{K}], \quad \pi(k) = \lim_{L \rightarrow \infty} \pi_L(k) = \inf_{\lambda > 0} \{\lambda k + \varphi(\lambda)\} = -\Sigma \left(1 - \frac{k}{\mathbb{K}}\right) \quad (26)$$

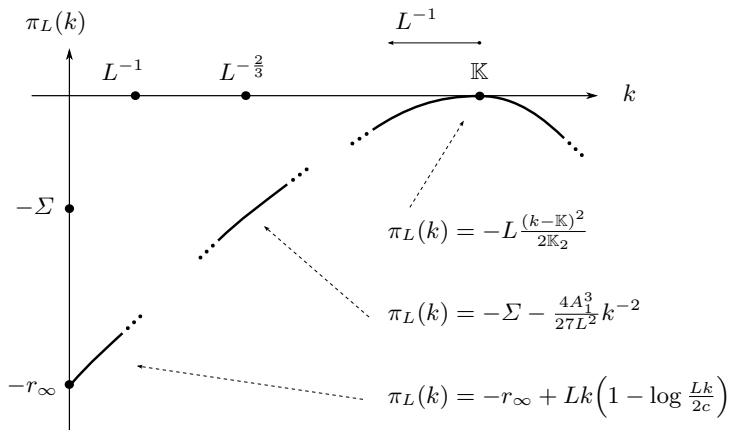


Fig. 7: Schematic plot of the finite-size scaling of the large deviation function $\pi_L(k) = \lim_{t \rightarrow \infty} \log \text{Prob}[K_t = tLk]$, deduced from the finite-size scaling of $\varphi_L(\lambda)$. The regime of smallest k ($k \ll L^{-1}$) corresponds to configurations with finite number of active sites. The intermediate regime ($L^{-\frac{2}{3}} \lesssim k \ll K - L^{-1}$) corresponds to the regime of phase transition, where the large deviation function is linear in the infinite size limit (cf. equation (40)). The picture for an unconstrained dynamics ($C_i = 1$ in (1-2)) has a completely different large deviation scaling $\pi_L^{\text{unc}}(k) = L\pi_1^{\text{unc}}(k)$ with inactive histories exponentially much less likely.

where φ is defined in (7). This follows from a simple computation (see [30] for a review on ldf in physics and mathematics). Note that negative activities cannot be produced. The physical picture behind the linear behaviour (26) is a two step mechanism. An activity deviation of order kt over the time interval $[0, t]$ is produced by first blocking the system in an inactive state during a time $(1 - \frac{k}{K})t$ and then letting the system in the stationary state (with mean activity K) during a time $\frac{k}{K}t$. This leads to an exponential cost $\Sigma(1 - \frac{k}{K})t$. We stress the fact that the switch from the inactive to the active state occurs on time scales much smaller than t and therefore has no impact on the large deviation function obtained in the large t limit. This behaviour is characteristic of a first order phase transition between the active and inactive regime. We examine below the consequences of the finite size corrections to the large deviations within both regimes. Results are summarised on figure 7.

The active regime:

For activities larger than K , the scaling is different as the constraints do not play a major role and the behaviour is similar to non-constrained systems, one has

$$\forall k > K, \quad \hat{\pi}(k) = \lim_{L \rightarrow \infty} \frac{1}{L} \pi_L(k) = \inf_{s < 0} \left\{ sk + \hat{\psi}(s) \right\}, \quad (27)$$

where $\hat{\psi}(s) = \lim_{L \rightarrow \infty} \frac{1}{L} \psi_L(s)$ which leads to

$$\forall k > K, \quad \text{Prob}[K_t \simeq tLk] \underset{t \rightarrow \infty}{\sim} e^{tL\hat{\pi}(k)} \quad (28)$$

In particular $\hat{\pi}$ is expected to be a smooth function for $k > 0$

$$\forall k > K, \quad \hat{\pi}(k) = -\frac{1}{2K_2} (k - K)^2 + O((k - K)^3) \quad (29)$$

where $\mathbb{K}_2 = \frac{1}{L^2} \langle K_t^2 \rangle_c$ is the variance of the activity.

The finite size scaling asserts that the transition for $\psi_L(s)$ takes place away from $s = 0$ and therefore, we expect that for very small deviations of the activity below \mathbb{K} , $L\hat{\pi}$ approximates the large deviation function $\pi_L(k) = \inf_{\lambda>0} \{\lambda k + \varphi_L(\lambda)\}$. This would hold only for $s > \frac{\lambda_c}{L}$, i.e. $k - \mathbb{K} \approx \frac{1}{L}$ (by optimising in (27)). This means that in a small window around \mathbb{K} of order $\frac{1}{L}$, the large deviations are of the form (29)

$$\pi_L(k) = -\frac{L}{2\mathbb{K}_2} (k - \mathbb{K})^2 + O(L^{-2}) \quad (30)$$

The inactive regime:

In the inactive regime, the finite size scaling takes into account the deviations of the width of the active droplet which will contribute to the activity deviations when k is close to 0. The finite size Legendre transform (26) reads

$$\forall k \in [0, \mathbb{K}], \quad \pi_L(k) = \inf_{\lambda>0} \{\lambda k + \varphi_L(\lambda)\} \quad (31)$$

where the optimal λ is given by $k = -\varphi'_L(\lambda)$. The finite size scaling (11) is valid for $\lambda \gg \lambda_c$

$$\varphi_L(\lambda) = -\Sigma - A_1 \left(\frac{\lambda}{L}\right)^{2/3} \quad \Rightarrow \quad k = \frac{2}{3} \frac{A_1}{L^{2/3}} \lambda^{-1/3} \quad (32)$$

This allows to estimate $\pi_L(k)$ for $k \approx \frac{1}{L} \lambda^{-1/3}$ and $\lambda \gg 1$

$$\pi_L(k) \simeq -\Sigma - \frac{4A_1^3}{27} \frac{1}{L^2 k^2} \quad (33)$$

This scaling should remain correct if the droplet width is very large microscopically, i.e. for $k \gg 1/L$. For $k \approx L^{-2/3} \lambda^{-1/3}$ with λ close to zero, the probability of observing an active droplet of width kL should vanish exponentially fast with a rate given by (33). But we will see below that these larger droplets do not contribute to $\pi_L(k)$.

The intermediate regime:

We consider now the intermediate deviations in k . The two-step mechanism described earlier has to be slightly modified to take into account the finite size corrections found in the active and inactive regimes (30), (33). Thus one expects that

$$\text{Prob}[K_t \simeq tL k] \underset{t \rightarrow \infty}{\sim} \sup_{\substack{k_1, k_2 \\ x_1, x_2}} \left\{ \exp \left(-tx_1 \frac{L}{2\mathbb{K}_2} (k_1 - \mathbb{K})^2 - tx_2 \left[\Sigma + \frac{4A_1^3}{27} \frac{1}{L^2 k_2^2} \right] \right) \right\} \quad (34)$$

where the supremum is taken over the activities k_1, k_2 and x_1, x_2 such that

$$1 = x_1 + x_2, \quad k = x_1 k_1 + x_2 k_2 \quad (35)$$

Suppose that $k \ll \mathbb{K} - \frac{1}{L}$. As $k_1 - \mathbb{K}$ is at most of order $1/L$, one can neglect the deviations with respect to k_1 and set $k_1 = \mathbb{K}$. This leads to optimise over k_2 with

$$k_1 = \mathbb{K}, \quad x_1 = 1 - x_2, \quad x_2 = \frac{\mathbb{K} - k}{\mathbb{K} - k_2} \in [0, 1] \quad (36)$$

Thus (34) reads

$$\text{Prob}[K_t \simeq tL k] \underset{t \rightarrow \infty}{\sim} \exp\left(-t(\mathbb{K} - k) \inf_{k_2 \leq k} \{G(k_2)\}\right) \quad (37)$$

where

$$G(k_2) = \frac{1}{\mathbb{K} - k_2} \left[\Sigma + \frac{4A_1^3}{27} \frac{1}{L^2 k_2^2} \right]. \quad (38)$$

The function G reaches its minimum for

$$k^* = \frac{\left(\sqrt{A^2 L^6 \Sigma^3 (A + \mathbb{K}^2 L^2 \Sigma)} + A \mathbb{K} L^4 \Sigma^2\right)^{2/3} - AL^2 \Sigma}{L^2 \Sigma^3 \sqrt{\sqrt{A^2 L^6 \Sigma^3 (A + \mathbb{K}^2 L^2 \Sigma)} + A \mathbb{K} L^4 \Sigma^2}} \underset{L \rightarrow \infty}{\sim} \left(\frac{2A}{\Sigma}\right)^{1/3} \frac{1}{L^{2/3}} \quad (39)$$

with $A = \frac{4A_1^3}{27}$. Finally we get

$$\lim_{t \rightarrow \infty} \frac{1}{t} \log \text{Prob}[K_t \simeq tL k] = \begin{cases} -(\mathbb{K} - k) G(k^*), & \text{for } k^* < k \ll \mathbb{K} - \frac{1}{L} \\ -(\mathbb{K} - k) G(k), & \text{for } \frac{1}{L} \ll k < k^* \end{cases} \quad (40)$$

Thus for a deviation $k > k^*$, the active droplet (in the inactive phase) has a microscopic width located around Lk^* and the large deviation is still linear with minor corrections compared to the limiting case. For $k < k^*$ then the system remains all the time in the inactive phase ($x_2 = 1$) and the droplet width shrinks leading to a non-linear large deviation cost in k . The fact that larger droplet widths cannot be observed in the large deviations is due to the first order phase transition.

The very inactive regime:

For $s \rightarrow \infty$ (*i.e.* $\lambda \gg L$) a single remaining site is active and one obtains the following asymptotics [6]:

$$\psi_L(s) = -r_\infty + 2ce^{-s} + O(e^{-s}) \quad \text{for } s \rightarrow \infty \text{ (i.e. } \lambda \gg L) \quad (41)$$

where $r_\infty = 2c$ is the mean escape rate in the configuration with one active site. Performing the inverse Legendre transform, this implies that

$$\pi_L(k) = -r_\infty + Lk \left(1 - \log \frac{Lk}{2c}\right) \quad \text{for } k \ll L^{-1} \quad (42)$$

5 Conclusion

We have shown that the dynamical phase coexistence occurring in the Fredrickson-Andersen model for histories at small positive s is well described by two Brownian interfaces enclosing an island (or “space-time bubble” [13]) of activity of width $L^{\frac{1}{3}}$ in a system of size L . The scaling of this physical picture is reflected in the finite size scaling of the dynamical free energy $\psi_L(s)$ of the model. We expect the same picture to be valid for a wider class of one-dimensional kinetically constrained models where the particle number is not conserved. It would be interesting to investigate the relation between our result and the statistics of large inactive bubbles in the non-modified ($s = 0$) dynamics.

In general, the finite size scaling exponents depend on the dimension and on the nature of the constraints [8]. Thus it would be interesting to extend our study to more general dynamics, in particular, to understand the interface fluctuations

in higher dimensional models. This would be key to connect our approach to realistic glass formers. The quantitative link between those realistic (in general, atomistic) models and kinetically constrained models have been explored in a variety of studies [31, 32, 33, 34]. Although it is beyond the scope of this article to use this correspondence to provide quantitative predictions on activity large deviation function in realistic models, we expect that the finite-size scaling exponents are related to geometrical features of inactive regions (see [12] for an example of such exponent).

Acknowledgements We would like to thank Frédéric van Wijland for useful discussions, and Christophe Berthod and Thierry Giamarchi for the Mafalda cluster at DPMC, University of Geneva, where part of the simulations were run. T.B., V.L. and C.T. acknowledge funding from ANR SHEPI and C.T. from ERC Advanced Grant PTRELSS 228032.

A Scaling of $\psi_L(s)$ in the interface model

We determine in this appendix the finite size corrections to the function $\hat{\varphi}_L(\lambda)$, defined in (9), in the effective interface description discussed in part 2.2. Let us first focus on a system with one boundary $x(t)$ between the active and inactive regions. It performs a random walk of jump rate p (resp. q) to the left (resp. right), starting from $x = 0$ at time 0, and constrained to come back to 0 at final time t . The walk $x(t)$ is reflected at 0 so that $x(t) \geq 0$. Appropriate values of p and q are discussed in section 4.1. The computation is done for generic values of p and q .

In the original model, the cost of maintaining the interface (that is, for $x(\tau)$ to come back in 0 at time $\tau = t$) is given by the surface tension Σ . In this effective description

$$Z_{\text{eff}}(s, t) \equiv \frac{\left\langle e^{-s\mathbb{K} \int_0^t d\tau x(\tau)} \delta(x(t) = 0) \right\rangle_{p,q}}{\langle \delta(x(t) = 0) \rangle_{p,q}} \quad (43)$$

where $\mathbb{K} = 4c^2(1 - c)$ is the mean density of activity and $\langle \cdot \rangle_{p,q}$ denotes the average on trajectories $x(\tau)_{0 \leq \tau \leq t}$ without constraint at final time. The normalisation $\langle \delta(x(t) = 0) \rangle_{p,q}$ is e.g. fixed from $Z_{\text{eff}}(0, t) = 1$.

Let us denote by $P(x, X, t)$ the probability of being in x at time t , having observed a value X of the area $\int_0^t d\tau x(\tau)$. The initial condition is $P(x, X, 0) = \delta_{x,0} \delta(X)$. Defining $\hat{P}(x, s, t) = \int dX e^{-s\mathbb{K}X} P(x, X, t)$, one has (using the constraint at final time $x(t) = 0$):

$$Z_{\text{eff}}(s, t) = \frac{\hat{P}(0, s, t)}{\hat{P}(0, 0, t)} \quad (44)$$

Moreover, from Feynman-Kac formula, the time evolution of $\hat{P}(x, s, t)$ is given by

$$\partial_t \hat{P}(x, s, t) = p \hat{P}(x+1, s, t) + q \hat{P}(x-1, s, t) - (p+q) \hat{P}(x, s, t) - s\mathbb{K}x \hat{P}(x, s, t) \quad (45)$$

and a reflection at $x = 0$. To symmetrize the walk, we now set $\hat{Q}(x, s, t) = (q/p)^{\frac{x}{2}} \hat{P}(x, s, t)$.

One has again $Z_{\text{eff}}(s, t) = \frac{\hat{Q}(0, s, t)}{\hat{Q}(0, 0, t)}$ and the evolution of $\hat{Q}(x, s, t)$ writes

$$\begin{aligned} \partial_t \hat{Q}(x, s, t) = & \sqrt{pq} \left[\hat{Q}(x+1, s, t) + \hat{Q}(x-1, s, t) - 2\hat{Q}(x, s, t) \right] \\ & - s\mathbb{K}x \hat{Q}(x, s, t) + (2\sqrt{pq} - p - q) \hat{Q}(x, s, t) \end{aligned} \quad (46)$$

The normalisation has changed but we see that apart from the constant loss rate $(2\sqrt{pq} - p - q)$, \hat{Q} describes a *symmetric* walk with the same term $s\mathbb{K}x \hat{Q}(x, s, t)$ corresponding to weighting trajectories by the area $\int_0^t d\tau x(\tau)$. In other words, defining at last $\tilde{Q}(x, s, t) = \hat{Q}(x, s, t) e^{-t(2\sqrt{pq} - p - q)}$, one has

$$Z_{\text{eff}}(s, t) = \frac{\tilde{Q}(0, s, t)}{\tilde{Q}(0, 0, t)} \quad (47)$$

and from the equation of evolution

$$\partial_t \tilde{Q}(x, s, t) = \sqrt{pq} \left[\tilde{Q}(x+1, s, t) + \tilde{Q}(x-1, s, t) - 2\tilde{Q}(x, s, t) \right] - s\mathbb{K}x\tilde{Q}(x, s, t) \quad (48)$$

we see that $\tilde{Q}(0, 0, t)$ does not increase exponentially in time since for $s = 0$ the equation describes a simple symmetric random walk. Moreover, in the large size limit ($s \rightarrow 0$), the evolution of $\tilde{Q}(x, s, t)$ is governed by the continuous in space operator

$$\sqrt{pq}\partial_x^2 - s\mathbb{K}x = 2\sqrt{pq} \left[\frac{1}{2}\partial_x^2 - \frac{s\mathbb{K}}{2\sqrt{pq}}x \right] \quad (49)$$

with reflecting boundary condition in 0. For bridges, the spectrum is known and its largest eigenvalue is given by [23]

$$\psi_{\text{eff}}^{\text{non-per}}(s) = 2\sqrt{pq} \left(\frac{s\mathbb{K}}{2\sqrt{pq}} \right)^{\frac{2}{3}} 2^{-\frac{1}{3}}\alpha_1 \quad (50)$$

where $\alpha_1 \approx 2.3381\dots$ is the first zero of the Airy function on the negative real axis. In periodic boundary conditions, one has two interfaces and the equivalent jump rates are multiplied by 2. Finally, this gives in the $s \rightarrow 0$ limit:

$$\psi_{\text{eff}}^{\text{per}}(s) = 4\sqrt{pq} \left(\frac{s\mathbb{K}}{4\sqrt{pq}} \right)^{\frac{2}{3}} 2^{-\frac{1}{3}}\alpha_1 \quad (51)$$

B A generic identity between large deviation functions

In this appendix we prove an identity used in part 3.2 between large deviation functions associated to the activity K_t and to the escape rate R_t defined below. We consider a Markov process on a finite number of configurations $\{\mathcal{C}\}$, with transition rates $W(\mathcal{C} \rightarrow \mathcal{C}')$ between configurations. The activity K_t is an history-dependent observable increasing by 1 upon jumping from \mathcal{C} to \mathcal{C}' . The probability $P(\mathcal{C}, K, t)$ of being in \mathcal{C} at time t having observed a value K of the observable K_t thus evolves in time through

$$\partial_t P(\mathcal{C}, K, t) = \sum_{\mathcal{C}'} W(\mathcal{C}' \rightarrow \mathcal{C}) P(\mathcal{C}', K-1, t) - r(\mathcal{C}) P(\mathcal{C}, K, t) \quad (52)$$

with $r(\mathcal{C}) = \sum_{\mathcal{C}'} W(\mathcal{C} \rightarrow \mathcal{C}')$ the escape rate from configuration \mathcal{C} . The Laplace transform $P(\mathcal{C}, s, t) = \sum_K e^{-sK} P(\mathcal{C}, K, t)$ verifies

$$\partial_t P(\mathcal{C}, s, t) = \sum_{\mathcal{C}'} e^{-s} W(\mathcal{C}' \rightarrow \mathcal{C}) P(\mathcal{C}', s, t) - r(\mathcal{C}) P(\mathcal{C}, s, t) \quad (53)$$

The cumulant generating function $\psi(s)$ defined in the infinite time limit as $\langle e^{-sK_t} \rangle \sim e^{t\psi(s)}$ is the largest eigenvalue of the operator \mathbb{W}_s of elements

$$(\mathbb{W}_s)_{\mathcal{C}\mathcal{C}'} = e^{-s} W(\mathcal{C}' \rightarrow \mathcal{C}) - r(\mathcal{C})\delta_{\mathcal{C}\mathcal{C}'} \quad (54)$$

since $\langle e^{-sK_t} \rangle = \sum_{\mathcal{C}} P(\mathcal{C}, s, t)$. Both K_t and $R_t = \int_0^t d\tau r(\mathcal{C}(\tau))$ quantify the activity of the histories. Their large deviation functions (ldf) are closely related. Indeed, let's consider the joint ldf

$$\Psi(s, \sigma) = \lim_{t \rightarrow \infty} \frac{1}{t} \log \langle e^{-sK_t - \sigma R_t} \rangle \quad (55)$$

As previously, one checks that $\Psi(s, \sigma)$ is given by the maximum eigenvalue of the operator $\mathbb{W}_{s, \sigma}$ of elements [7]

$$(\mathbb{W}_{s, \sigma})_{\mathcal{C}\mathcal{C}'} = e^{-s} W(\mathcal{C}' \rightarrow \mathcal{C}) - (1 + \sigma)r(\mathcal{C})\delta_{\mathcal{C}\mathcal{C}'} \quad (56)$$

It verifies the symmetry $\mathbb{W}_{s, \sigma} = (1 + \sigma)\mathbb{W}_{s + \log(1 + \sigma), 0}$ and so does the ldf:

$$\Psi(s, \sigma) = (1 + \sigma)\Psi(s + \log(1 + \sigma), 0) \quad (57)$$

Besides, the mean values of K_t and R_t in the s -state are given by

$$\frac{1}{t}\langle K_t \rangle_s = -\partial_s \Psi(s, \sigma)|_{\sigma=0} \quad \frac{1}{t}\langle R_t \rangle_s = -\partial_\sigma \Psi(s, \sigma)|_{\sigma=0} \quad (58)$$

Differentiating the symmetry (57) with respect to σ and sending σ to 0, one gets

$$\partial_\sigma \Psi(s, \sigma)|_{\sigma=0} = \Psi(s, 0) + \partial_s \Psi(s, \sigma)|_{\sigma=0} \quad (59)$$

which implies

$$\psi(s) = \frac{1}{t}\langle K_t \rangle_s - \frac{1}{t}\langle R_t \rangle_s \quad (60)$$

This relation is generic. It leads to the relation (14) between scaling exponents for the FA model in the inactive regime $s = \lambda/L$.

C Bernoulli approximation to determine $\varphi_L(\lambda)$

In this appendix, we obtain the expression of the Courant-Fischer optimisation principle of part 3.3 for Bernoulli states. Before this, one needs to symmetrize the evolution operator \mathbb{W}_s introduced in (54). We take the notation of appendix B. Assuming that the jump rates verify the detailed balance symmetry $W(\mathcal{C} \rightarrow \mathcal{C}')P_{\text{eq}}(\mathcal{C}) = W(\mathcal{C}' \rightarrow \mathcal{C})P_{\text{eq}}(\mathcal{C}')$, it is generically possible to symmetrize the operator of evolution \mathbb{W}_s through the similarity transformation $\mathbb{W}_s^{\text{sym}} \equiv \hat{P}_{\text{eq}}^{-\frac{1}{2}} \mathbb{W}_s \hat{P}_{\text{eq}}^{\frac{1}{2}}$, where \hat{P}_{eq} is the diagonal operator of elements $P_{\text{eq}}(\mathcal{C})$. Upon symmetrisation, we have that $\psi(s)$ is also the largest eigenvalue of the symmetric operator $\mathbb{W}_s^{\text{sym}}$ of elements

$$(\mathbb{W}_s^{\text{sym}})_{\mathcal{C}\mathcal{C}'} = e^{-s} [W(\mathcal{C}' \rightarrow \mathcal{C})W(\mathcal{C} \rightarrow \mathcal{C}')]^{\frac{1}{2}} - r(\mathcal{C})\delta_{\mathcal{C}\mathcal{C}'} \quad (61)$$

It is convenient to represent the operator of evolution in terms of spin $\frac{1}{2}$ operators σ^\pm and \hat{n} . On each site i , σ^\pm is the creation/annihilation operator and \hat{n} is the counting operator. They are defined by

$$\sigma^+|0\rangle = |1\rangle \quad \sigma^-|0\rangle = 0 \quad \hat{n}|0\rangle = 0 \quad (62)$$

$$\sigma^+|1\rangle = 0 \quad \sigma^-|1\rangle = |0\rangle \quad \hat{n}|1\rangle = |1\rangle \quad (63)$$

Where $|0\rangle$ and $|1\rangle$ are the vectors for empty and occupied states. One has

$$\mathbb{W}_s = \sum_{1 \leq i \leq L} \left[e^{-s} (c\sigma_i^+ + (1-c)\sigma_i^-) - c(1-\hat{n}_i) - (1-c)\hat{n}_i \right] (\hat{n}_{i+1} + \hat{n}_{i-1}) \quad (64)$$

Transition rates obey detailed balance with respect to the product Bernoulli measure of uniform density c (conditioned to exclude the fully inactive configuration). The symmetrized operator of evolution writes

$$\mathbb{W}_s^{\text{sym}} = \sum_{1 \leq i \leq L} \left[e^{-s} \sqrt{c(1-c)} (\sigma_i^+ + \sigma_i^-) - c(1-\hat{n}_i) - (1-c)\hat{n}_i \right] (\hat{n}_{i+1} + \hat{n}_{i-1}) \quad (65)$$

Defining the vector $|\rho\rangle$ corresponding to the Bernoulli distribution of density $\sqrt{\rho}$:

$$|\rho\rangle = \sqrt{\rho}|1\rangle + (1-\sqrt{\rho})|0\rangle \quad (66)$$

and taking $|X\rangle$ in (17) to be the state $|\rho_1 \dots \rho_L\rangle^{\text{cond}}$ conditioned to exclude the fully empty configuration:

$$|\rho_1 \dots \rho_L\rangle^{\text{cond}} = \sum_{n_i: \sum_i n_i \neq 0} \langle n_1 \dots n_L | \rho_1 \dots \rho_L \rangle |n_1 \dots n_L\rangle \quad (67)$$

one obtains (18) by direct computation.

References

1. Ludovic Berthier and Giulio Biroli. [Theoretical perspective on the glass transition and amorphous materials](#). *Rev. Mod. Phys.* **83**, 587 (2011).
2. Felix Ritort and Peter Sollich. [Glassy dynamics of kinetically constrained models](#). *Adv. Phys.* **52**, 219 (2003).
3. Juan P. Garrahan, Peter Sollich, and Cristina Toninelli. [Kinetically constrained models](#). [arXiv:1009.6113](#) and Chapter of “*Dynamical heterogeneities in glasses, colloids, and granular media*”, Eds.: L. Berthier, G. Biroli, J-P Bouchaud, L. Cipelletti and W. van Saarloos (Oxford University Press, 2011) (2010).
4. Mauro Merolle, Juan P. Garrahan, and David Chandler. [Space-time thermodynamics of the glass transition](#). *PNAS* **102**, 10837 (2005).
5. Vivien Lecomte, Cécile Appert-Rolland, and Frédéric Wijland. [Thermodynamic formalism for systems with markov dynamics](#). *J. Stat. Phys.* **127**, 51 (2007).
6. Juan P. Garrahan, Robert L. Jack, Vivien Lecomte, Estelle Pitard, Kristina van Duivendijk, and Frédéric van Wijland. [Dynamical First-Order phase transition in kinetically constrained models of glasses](#). *Phys. Rev. Lett.* **98**, 195702 (2007).
7. Juan P. Garrahan, Robert L. Jack, Vivien Lecomte, Estelle Pitard, Kristina van Duivendijk, and Frédéric van Wijland. [First-order dynamical phase transition in models of glasses: an approach based on ensembles of histories](#). *J. Phys. A* **42**, 075007 (2009).
8. Thierry Bodineau and Cristina Toninelli. [Activity phase transition for constrained dynamics](#). [arXiv:1101.1760](#), accepted for publication in *Comm. Math. Phys.*, doi:10.1007/s00220-012-1449-4 (2011).
9. Christian Maes, Karel Netočný, and Bram Wynants. [On and beyond entropy production: the case of markov jump processes](#). *Markov Proc. Rel. Fields* **14**, 445 (2008).
10. Lester O. Hedges, Robert L. Jack, Juan P. Garrahan, and David Chandler. [Dynamic Order-Disorder in atomistic models of structural glass formers](#). *Science* **323**, 1309 (2009).
11. Thierry Bodineau and Raphaël Lefevere. [Large deviations of lattice hamiltonian dynamics coupled to stochastic thermostats](#). *J. Stat. Phys.* **133**, 1 (2008).
12. Estelle Pitard, Vivien Lecomte, and Frédéric Van Wijland. [Dynamic transition in an atomic glass former: a molecular dynamics evidence](#). *Europhys. Lett.* **96**, 184207 (2011).
13. David Chandler and Juan P. Garrahan. [Dynamics on the way to forming glass: Bubbles in Space-Time](#). *Ann. Rev. Phys. Chem.* **61**, 191 (2010).
14. Robert L. Jack, Juan P. Garrahan, and David Chandler. [Space-time thermodynamics and subsystem observables in a kinetically constrained model of glassy materials](#). *J. Chem. Phys.* **125**, 184509 (2006).
15. Cécile Appert-Rolland, Bernard Derrida, Vivien Lecomte, and Frédéric van Wijland. [Universal cumulants of the current in diffusive systems on a ring](#). *Phys. Rev. E* **78**, 021122 (2008).
16. Vivien Lecomte, Alberto Imparato, and Frédéric van Wijland. [Current fluctuations in systems with diffusive dynamics, in and out of equilibrium](#). *Prog. Theor. Phys. Suppl.* **184**, 276 (2010).
17. Mieke Gorissen and Carlo Vanderzande. [Finite size scaling of current fluctuations in the totally asymmetric exclusion process](#). *J. Phys. A* **44**, 115005 (2011).
18. Thierry Bodineau and Bernard Derrida. [Distribution of current in nonequilibrium diffusive systems and phase transitions](#). *Phys. Rev. E* **72**, 066110 (2005).
19. Lorenzo Bertini, Alberto De Sole, Daniele Gabrielli, Giovanni Jona-Lasinio, and Claudio Landim. [Non equilibrium current fluctuations in stochastic lattice gases](#). *J. Stat. Phys.* **123**, 237 (2006).
20. Glenn H. Fredrickson and Hans C. Andersen. [Kinetic ising model of the glass transition](#). *Phys. Rev. Lett.* **53**, 1244 (1984).
21. Ostap Hryniv and Yvan Velenik. [Universality of critical behaviour in a class of recurrent random walks](#). *Probab. Theory Relat. Fields* **130**, 222 (2004).
22. Yvan Velenik. [Entropic repulsion of an interface in an external field](#). *Probab. Theory Relat. Fields* **129**, 83 (2004).
23. Satya N. Majumdar and Alain Comtet. [Airy distribution function: From the area under a brownian excursion to the maximal height of fluctuating interfaces](#). *J. Stat. Phys.* **119**, 777 (2005).
24. Vivien Lecomte and Julien Tailleur. [A numerical approach to large deviations in continuous time](#). *J. Stat. Mech.* **P03004** (2007).
25. Julien Tailleur and Vivien Lecomte. [Simulation of large deviation functions using population dynamics](#). *AIP Conf. Proc.* **1091**, 212 (2009).
26. Cristian Giardinà, Jorge Kurchan, and Luca Peliti. [Direct evaluation of Large-Deviation functions](#). *Phys. Rev. Lett.* **96**, 120603 (2006).

-
27. Cristian Giardinà, Jorge Kurchan, Vivien Lecomte, and Julien Tailleur. [Simulating rare events in dynamical processes](#). *J. Stat. Phys.* **145**, 787 (2011).
 28. Pablo I. Hurtado and Pedro L. Garrido. [Current fluctuations and statistics during a large deviation event in an exactly solvable transport model](#). *J. Stat. Mech.* **P02032** (2009).
 29. Francesco Turci and Estelle Pitard. [Large deviations and heterogeneities in a driven kinetically constrained model](#). *Europhys. Lett.* **94**, 10003 (2011).
 30. Hugo Touchette. [The large deviation approach to statistical mechanics](#). *Phys. Rep.* **478**, 1 (2009).
 31. Juan P. Garrahan and David Chandler. [Geometrical explanation and scaling of dynamical heterogeneities in glass forming systems](#). *Physical Review Letters* **89**, 035704 (2002).
 32. Ludovic Berthier, Giulio Biroli, Jean-Philippe Bouchaud, Walter Kob, Kunimasa Miyazaki, and David R. Reichman. [Spontaneous and induced dynamic correlations in glass formers. II. model calculations and comparison to numerical simulations](#). *The Journal of Chemical Physics* **126**, 184504 (2007).
 33. Raphaël Candelier, Asaph Widmer-Cooper, Jonathan K. Kummerfeld, Olivier Dauchot, Giulio Biroli, Peter Harrowell, and David R. Reichman. [Spatiotemporal hierarchy of relaxation events, dynamical heterogeneities, and structural reorganization in a supercooled liquid](#). *Physical Review Letters* **105**, 135702 (2010).
 34. Aaron Keys, Lester Hedges, Juan Garrahan, Sharon Glotzer, and David Chandler. [Excitations are localized and relaxation is hierarchical in Glass-Forming liquids](#). *Physical Review X* **1**, 021013 (2011).